J Mater Sci: Mater Electron

Effect of Cu interlayer on opto-electrical parameters of ZnO thin films

S. S. Fouad[1], B. Parditka[2], M. Nabil[3,*], E. Baradács[2,4], S. Negm[3], and Zoltán Erdélyi[2]

[1] *Department of Physics, Faculty of Education, Ain Shams University, Cairo 11566, Egypt*
[2] *Department of Solid-State Physics, Faculty of Sciences and Technology, University of Debrecen, P.O. Box 400, Debrecen 4002, Hungary*
[3] *Department of Basic Engineering Sciences, Faculty of Engineering (Shoubra), Benha University, Benha, Egypt*
[4] *Department of Environmental Physics, Faculty of Sciences and Technology, University of Debrecen, Poroszlay u. 6, Debrecen 4026, Hungary*

Received: 19 May 2022
Accepted: 1 August 2022

© The Author(s), under exclusive licence to Springer Science+Business Media, LLC, part of Springer Nature 2022

ABSTRACT

In this paper, we focused our attention on the tailoring of structure and optical analysis as a function of Cu interlayer between the ZnO layers. The Cu interlayer was deposited by magnetron sputtering, while the ZnO layers were deposited by atomic layer deposition. Morphological analysis, based on grazing incident X-ray diffraction patterns and scanning electron microscope images, revealed formation of crystalline phase and a successful incorporation of Cu into ZnO. The estimated average crystallite size increased from 8.64 to 12.05 nm as Cu interlayer thickness increased from 20 to 70 nm. The averaged value of the surface roughness was determined, from both the profilometer and the XRD measurements. The determinations of the optical band gap and the nature of optical transition were performed by the analysis of absorption spectrum. Also, some physical quantities, such as optical density OD and skin depth δ, were estimated. Optical absorption studies revealed that all the films have a direct allowed transition. A shift in the optical energy band gap E_g from 2.75 to 2.43 eV as a function of Cu interlayer thickness was observed. The linear refractive index (n) was analyzed to determine the metallization criterion M, the reflection loss function R_L, the transmission coefficient T and the relative density D_r. Moreover, we showed that the doping of ZnO with different thickness of Cu interlayer enhances its optical activity and electrical conductivity as well, which makes it useful for photocatalytic application and sensor device fabrication in particular conditions.

Address correspondence to E-mail: mohammed_diab35@yahoo.com

https://doi.org/10.1007/s10854-022-08871-w

Springer

Published online: 22 August 2022

1 Introduction

ZnO thin film exhibits a high refractive index and a wide band gap of ≈ 3.1 eV, which have attracted great attention due to its outstanding physical properties that can be applied in various fields such as gas sensors, solar cells, photodiodes and catalysts [1–3]. These applications are made possible by doping ZnO with various elements such as Cu, Ag, Fe and Mn. The unique properties of ZnO combined with metal were recently demonstrated to be an efficient approach for sensor device fabrication. The market transparent and conducting oxide (TCO) for oxide thin films prepared by different techniques is growing exponentially due to the wide range of potential applications [4, 5]. Atomic layer deposition (ALD) is a high-performance scalable layer-by-layer deposition technique that controls the deposition process and the concentration of thin films in the nanometer range to modulate structure and opto-electrical properties. ALD was developed to produce highly conformal pinhole-free insulating films and is particularly powerful in preparing multilayers with thickness controllability to be an efficient approach for electronic and optoelectronic devices [6–9]. The ALD is a promising deposition method which breaks the chemical vapor deposition (CVP) reaction. The optical absorption coefficient is a crucial parameter in determining the film efficiency under operational conditions [10–12]. As a matter of fact, a lot of studies have been made on ZnO/Cu/ZnO thin films, with 0–16 nm thick Cu layer due to its lower resistivity and high transmittance [13, 14]. In this work, three types of thin films were prepared in the form of ZnO/Cu/ZnO sandwich structure with constant (70 nm) ZnO thickness and variable sputtered Cu interlayer thickness (20, 50 and 70 nm) by ALD and magnetron sputtering techniques. The objective of this work is to study the effect of increasing the thickness of Cu interlayer on the optical properties and other related parameters.

2 Experimental procedures

Three types of sandwich structured samples were deposited with constant ZnO thickness and variable Cu interlayer thickness by ALD and dc magnetron sputtering, respectively, as follows: ZnO(70 nm)/Cu(20 nm, 50 nm, 70 nm)/ZnO(70 nm); from now on labeled as $ZC_{20}Z$, $ZC_{50}Z$ and $ZC_{70}Z$. (see Fig. 1) The magnetron sputtering process was carried out at room temperature with a base pressure of $\sim 5 \times 10^{-7}$ mbar, a working pressure of 7×10^{-3} mbar Ar and a sputtering power of 10 W. A Beneq TFS-200 was used for ALD in thermal mode using DEZ and H_2O as precursors. The pulse duration was 0.3 s for both precursors. The nitrogen purge between precursor pulses was 3 s. 420 ALD cycles were used. The deposition temperature was 200 °C, and the reactor pressure was 1.3 mbar. The film thickness of the three samples was precisely controlled through the number of ALD cycles and checked by a profilometer (AMBIOS XP-1) and a spectroscopic ellipsometer (Semilab SE-2000).

The phase and structure of $ZC_{20}Z$, $ZC_{50}Z$ and $ZC_{70}Z$ were identified using grazing incident X-ray diffraction (GIXRD, Rigaku Smart Lab). The morphology of the films was analyzed using a scanning electron microscope (SEM, Thermo Scientific Scios 2). The transmission and optical absorbance were measured using a V-670 Jasco double-beam spectrophotometer, which utilizes a unique, single monochromator design covering a wavelength range from 190 to 2700 nm. Experimentally, the absorption coefficient α can be calculated from the absorbance from this simple relation $\alpha = 2.303\ A/t$, where A is the absorbance and t is the thickness of thin film. All sample measurements were performed at room temperature.

3 Results and discussion

3.1 Structural characterization

Figure 2 shows the GIXRD pattern of $ZC_{20}Z$, $ZC_{50}Z$ and $ZC_{70}Z$, grown on Si(100) substrate. The GIXRD pattern for $ZC_{20}Z$ shows crystalline ZnO and Cu; moreover, some CuO is also present, which could be associated to the large affinity of Cu to O and the thin layer of Cu layer (20 nm only).

The GIXRD patterns of $ZC_{50}Z$ and $ZC_{70}Z$, seen in Fig. 2, show good similarity to the above described $ZC_{20}Z$, and the only difference that appears is the ratio among the intensity of the individual peaks; no peak disappears, and no new peak appears. The missing sharp peak at − 33 degree for $ZC_{50}Z$ belongs to the Si substrate and known as its forbidden reflection. The main peak of the substrate is tilted out,

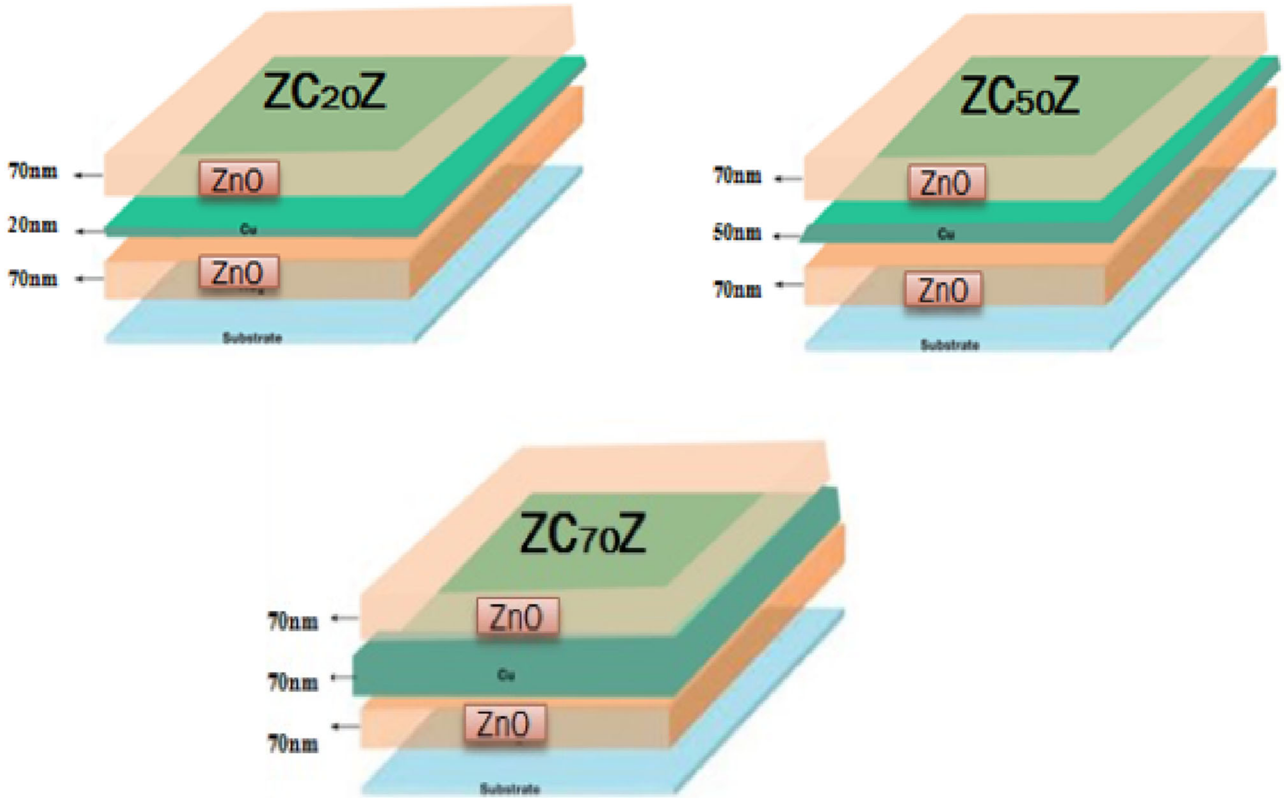

Fig. 1 Schematic drawing of $ZC_{20}Z$, $ZC_{50}Z$ and $ZC_{70}Z$ sandwich structures

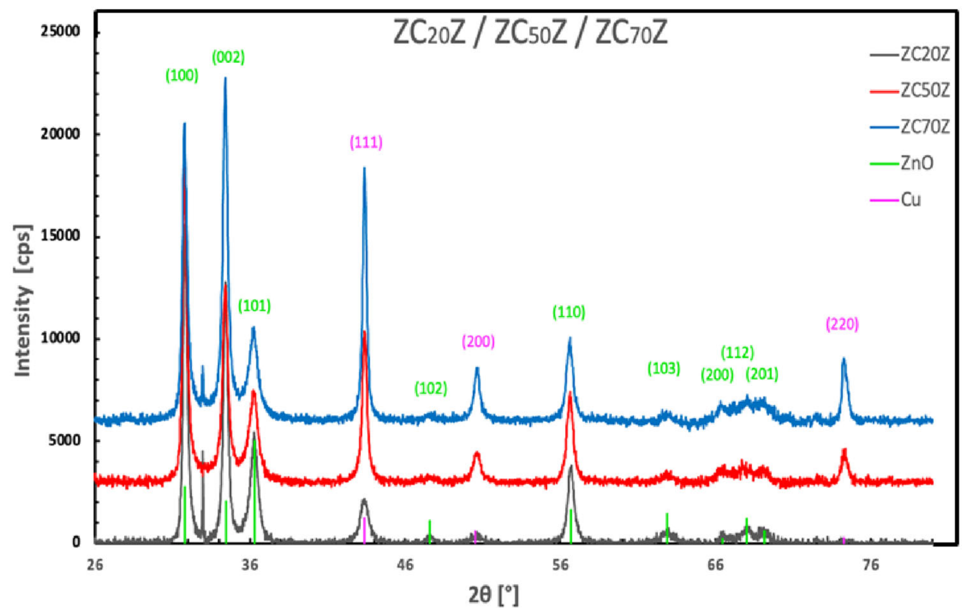

Fig. 2 GIXRD diffraction patterns of $ZC_{20}Z$, $ZC_{50}Z$ and $ZC_{70}Z$ thin films

however at certain rotation angles of the forbidden peak is visible [15]. The above chart shows the major advantages of the ALD technique over its competitors, i.e., chemical co-precipitation method [16], co-sputtering method [17] and RF simultaneous magnetron sputtering [18]. The observed increase in the intensity of the peak belongs to Cu(111) indicates that the preferential growth of the sputtered Cu interlayer

is strongly affected by the variation of the Cu thickness. Our results are in a good agreement with the data given in [19]. The crystallite sizes of the three samples were calculated from the GIXRD patterns and are given in details in Table 1. For further investigation, we also used the data measured by the spectroscopic ellipsometer and the profilometer, furthermore performed X-ray reflectivity (XRR) measurements. From these measurements, we were able to determine an average value of the surface roughness, $\pm$ 3 nm, and the results are summarized in Table 1.

As seen the roughness decreases from 3.0 ± 0.04 nm to 1.8 ± 0.02 nm with increasing the sputtered Cu interlayer thickness, therefore, the surface appears more uniform; moreover, the crystal size increases from 8.64 nm to 12.05 nm. The SEM images for the three types of samples seen in Fig. 3a–c are in accordance with these results. As can be seen in Fig. 3b and c, the $ZC_{50}Z$ and $ZC_{70}Z$ samples are uniform, continuous and have a homogeneous surface, while in Fig. 3a the Cu layer of $ZC_{20}Z$ shows segmented incomplete coverage.

In Fig. 3a, the dark spots show the lack of continuity of the Cu layer. The small grayish grains are the grains of the polycrystalline Cu layer in all three images. The insets show a larger area of the samples at lower magnification. The Cu layer is obscured by the topmost crystalline ZnO layer. The effect of scattering of incident light from rough surfaces reduces the transmittance; however, the transmittance of the three samples under study decreases as the surface roughness of the samples decreases, as shown in Fig. 4. In other words, the sample with a rougher surface is also thinner, and the transmittance increases exponentially with decreasing thickness, so this may compensate with the effect of roughness. The decrease in the optical transmission with the increase in Cu thickness is also observed in [19]. For further discussion, see also the absorption analysis in the next session.

3.2 Absorption analysis

The optical absorption measurements are helping to understand the band gap. The absorption coefficient determines how far into material light of a particular wavelength can penetrate before it is absorbed. Therefore, the absorption coefficient is described as the reciprocal of the depth of penetration of radiation into bulk solid. In any low absorption material, light is weakly absorbed, and if it is thin enough, it will appear transparent to that wavelength [20]. The significant enhancement of UV–V absorption spectra of $ZC_{20}Z$, $ZC_{50}Z$ and $ZC_{70}Z$ is given in Fig. 5. The experimental results show that the absorption is obviously affected by sputtered Cu interlayer thickness. The broad absorption band in the range 400 to 600 nm was attributed to multiple vibrionic excitations [21].

All spectra presented had similar absorption bands at around 500 to 600 nm. The strong absorption peaks around 375 to 425 nm are due to the fundamental band gap and high-energy critical point transitions. We can assume that the absorption in the UV region significantly depends on the sample structure. Surface roughness generally increases the optical absorption, as indicated in Table 2 as well as the absorption seen in Fig. 5. Optical density OD expresses the tendency of the atoms of a material to retain the absorbed energy, and it is the loss of intensity that occurs due to absorption and scattering when light passes through a medium. The value of the optical density is the negative logarithmic measurement of the transmission percentage $\{\%T\}$ and can be calculated by a simple equation $OD = \alpha t$ [22]. Figure 6 presents the variation of OD with the photon energy for the three samples under investigation.

The obtained OD from Fig. 6 demonstrates that the OD values increase with increasing the sputtered Cu interlayer thickness, which is in a good agreement with transmittance spectra of the three samples given in Fig. 4 and the root-mean-square values of the

Table 1 Crystallite size and the roughness of Cu for studied $ZC_{20}Z$, $ZC_{50}Z$ and $ZC_{70}Z$ thin films grown by ALD

Samples	$2\theta^{\circ}$ (Cu)	Radian (θ^0) (Cu)	Cos Radian (θ^0) (Cu)	β^0(FWHM)	Radian β^0	D Crystallite size (nm)	Roughness (nm)
$ZC_{20}Z$	43.48	0.3794	0.9289	0.99	0.017278	8.64	3.0 ± 0.04
$ZC_{50}Z$	43.432	0.3790	0.9290	0.737	0.012863	11.60	2.2 ± 0.09
$ZC_{70}Z$	43.466	0.3793	0.9289	0.71	0.012391	12.05	1.8 ± 0.02

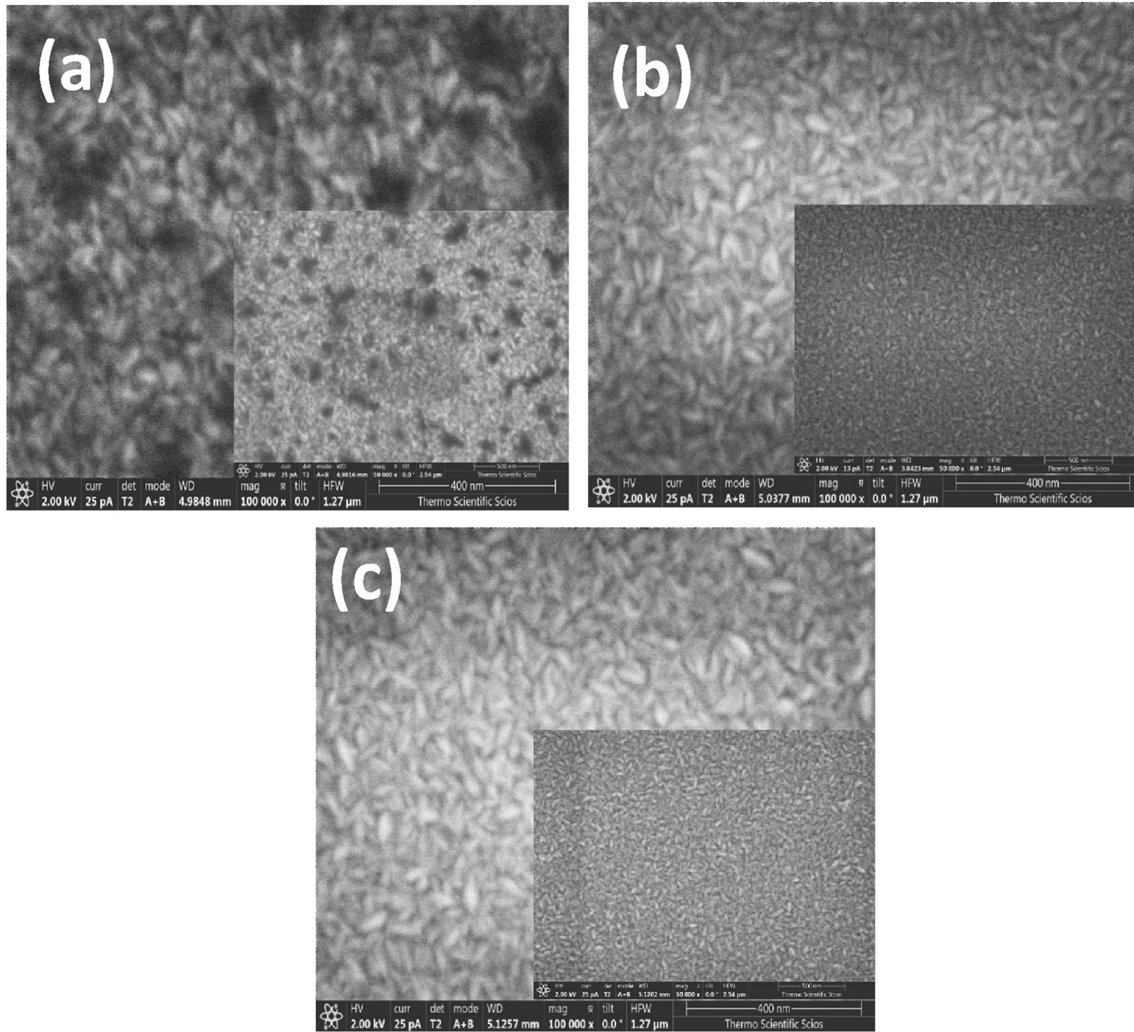

Fig. 3 Surface morphology of the **a** $ZC_{20}Z$, **b** $ZC_{50}Z$, **c** $ZC_{70}Z$ structure

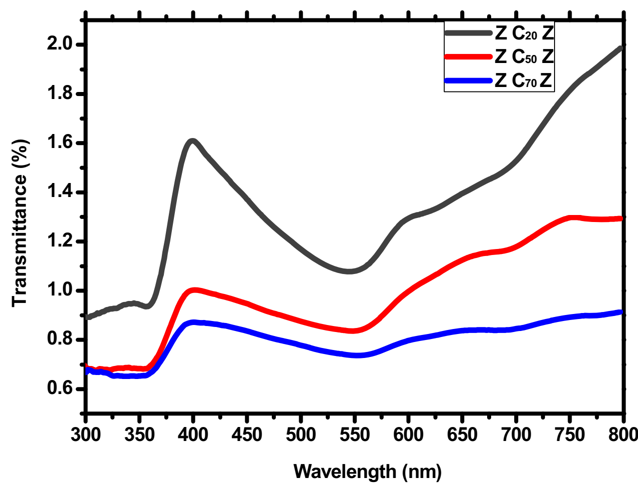

Fig. 4 Transmittance spectra of $ZC_{20}Z$, $ZC_{50}Z$ and $ZC_{70}Z$ thin films grown by ALD

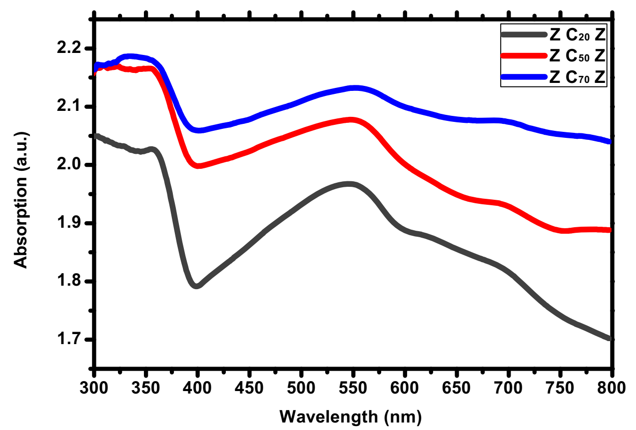

Fig. 5 Absorption spectra of $ZC_{20}Z$, $ZC_{50}Z$ and $ZC_{70}Z$ thin films grown by ALD

roughness listed in Table 1. The skin depth δ or the penetration depth is a measure of how deep light or

Table 2 Direct optical energy gap (E_g), average optical electronegativity ($\Delta\chi$), linear reflection index (n) for the studied $ZC_{20}Z$, $ZC_{50}Z$ and $ZC_{70}Z$ thin films grown by ALD

Samples	Band gap (E_g) (eV)	$\Delta\chi$	Equation of refractive index (n) $Eq(3)Eq(4)Eq(5)$		
$ZC_{20}Z$	2.75	0.739	2.42	1.822	2.471
$ZC_{50}Z$	2.63	0.706	2.45	1.925	2.505
$ZC_{70}Z$	2.43	0.653	2.50	2.095	2.577

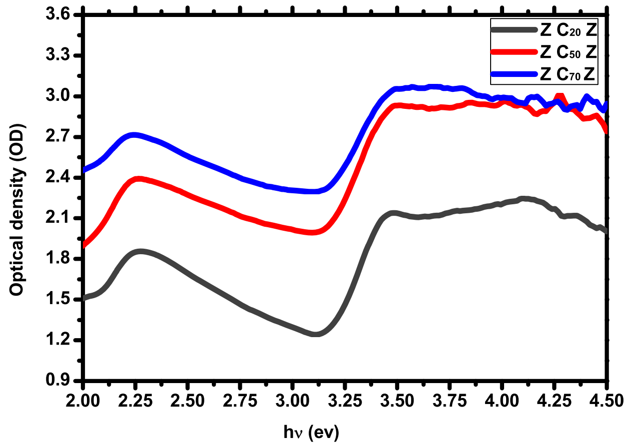

Fig. 6 Optical density of $ZC_{20}Z$, $ZC_{50}Z$ and $ZC_{70}Z$ thin films grown by ALD

any electromagnetic radiation can penetrate into a material. The skin depth is defined as the depth where current density is just about 37% of the value at surface. The effective depth of penetration is calculated by δ = 1/α [23]. The variations of the δ V_S $h\upsilon$ for various compositions are given in Fig. 7.

As seen, the maximum value of skin depth was obtained for the sputtered Cu interlayer thickness of 20 nm. The correlation between skin depth and optical properties is desirable as absorption loss depends on thickness and skin depth. Comparing Figs. 5 and 7, the inverse relation between the absorption and the skin depth is confirmed. In solid-state physics, the optical energy gap E_g is an energy range in a solid where no electron state exists. E_g is the energy required to promote a valence electron bound to an atom become a conduction electron; therefore, it is a major factor for determining the electrical conductivity and is strongly dependent upon the crystal structure of the material. The band gap is predominantly influenced by the crystallite size, and the spacing of the electronic level and the band gap decreases with increasing crystallite size.

In order to verify the optical band gap and the type of optical transition, an equation derived by the following relation shall be used [24–26].

$$\alpha h\nu = B(h\nu - E_g)^r \quad (1)$$

here B is the absorption constant, and r is the factor that detects the type of transition, where r can be ½ or 2 for direct and indirect optical transition. Considering Eq. 1, the best fit obtained for r was at r = ½, that is for allowed direct transition. The plotting of $(\alpha h\upsilon)^2$ versus $h\upsilon$ is shown in Fig. 8. The values of the direct

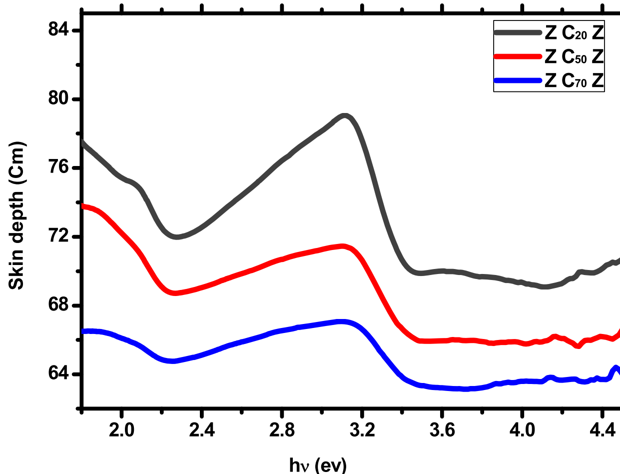

Fig. 7 Skin depth of $ZC_{20}Z$, $ZC_{50}Z$ and $ZC_{70}Z$ thin films grown by ALD

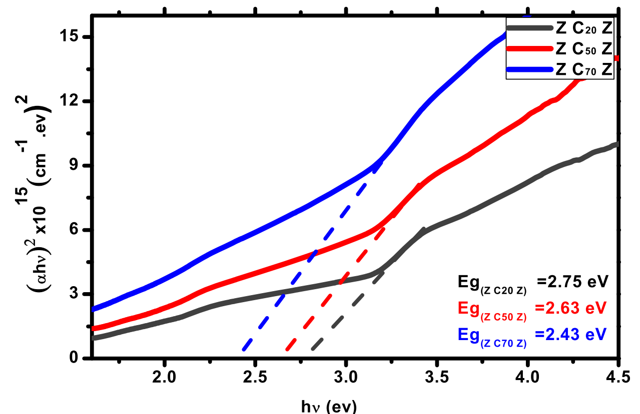

Fig. 8 Presents $(\alpha h\nu)^2$ versus $(h\nu)$ plot for $ZC_{20}Z$, $ZC_{50}Z$ and $ZC_{70}Z$ thin films grown by ALD

energy gap E_g were determined graphically for the three samples under study by intersecting the linear extrapolation of the absorption edge and are summarized in Table 2.

As seen, the E_g values were decreased from 2.75 to 2.43 eV by increasing the sputtered Cu interlayer thickness from 20 to70nm, which is consistent with the results reported elsewhere [27]. This decrease may be attributed to the increase in the defect centers. The correlation between the band gap and the crystallite size is confirmed, as the band gap decreases with increasing crystallite size, because the electron–hole pair is much wider (compare results in Tables 1, 2). The band gap is the minimum amount of energy required for an electron to break free of its bond state. The optical electronegativity $\Delta\chi$ is a key parameter to understand the chemical bonding [28].

$$E_g = 3.72(\Delta\chi) \quad (2)$$

As the electronegativity decreases as seen in Table 2, the energy difference between bonding and antibonding also decreases, leading to a decrease in E_g, as observed.

3.3 Refractive index (*n*)

The refractive indices (n) of $ZC_{20}Z$, $ZC_{50}Z$ and $ZC_{70}Z$ were calculated using three different equations based on the optical energy gap values E_g by [29, 30]:

$$n^4 E_g = 95\text{eV} \quad (3)$$

$$n = 4.16 - 0.85E_g \quad (4)$$

$$n = \frac{n^2 - 1}{n^2 + 2} = 1 - \sqrt{\frac{E_g}{20}} \quad (5)$$

The data are listed in Table 2. It can be seen that the trend of increasing refractive index with increasing Cu layer thickness was the same for the three equations, and that the refractive indices estimated from Eqs. 3 and 5 are nearly the same. We decided to take the average value of (n) given from Eqs. 3 and 5. The average values of the refractive index are presented in Table 3. The increase in the refractive index with increasing Cu layer thickness is related to the increase in the optical density of the sputtered Cu layers seen in Fig. 6.

Table 3 Average linear reflection index (n), correlation between molar volume (V_m) and molar refraction (R_m), metallization criterion (M), reflection loss (R_L), transmission coefficient (T) and relative density (D_r) for the studied $ZC_{20}Z$, $ZC_{50}Z$ and $ZC_{70}Z$ thin films grown by ALD

Samples	n (Average)	R_m/V_m	M	R_L	T	D_r (%)
$ZC_{20}Z$	2.237	0.536	0.464	0.145	0.745	74.84
$ZC_{50}Z$	2.477	0.631	0.369	0.180	0.694	95.98
$ZC_{70}Z$	2.538	0.644	0.356	0.188	0.682	101.70

3.4 Opto-electrical parameters

The relationship between the refractive index and opto-electrical parameters suggests that the parameters are predominantly influenced by any change in the refractive index. The correlation between molar volume V_m and molar refraction R_m is given by the relation [8]:

$$R_m/V_m = \left(n^2 - 1/n^2 + 2\right) \quad (6)$$

The ratio of R_m/V_m determines the sufficient conditions for predicting the nonmetallic or metallic character of the samples, which are R_m/V_m ‹1 (non-metal) and $R_m/V_m \geq 1$ (metal). The metallization criterion M is used to find out the metallic or non-metallic nature of the material and can be expressed by [31]:

$$M = 1 - (R_m/V_m) \quad (7)$$

The metallization criterion decreases with increasing sputtered Cu interlayer thickness as shown in Table 3. This decrease indicates that the samples are becoming more metallic. These results indicate that increasing sputtered Cu layer becomes near continuous to electron conduction and a large amount of current pass through it. The reflection loss R_L from the surface is an important new test parameter, and it is the ratio of reflected power to incident power and is given by the following equation [31]:

$$R_L = \left(\frac{n-1}{n+1}\right)^2 \quad (8)$$

As observed, R_L listed in Table 3 increases with increasing sputtered Cu interlayer thickness. The transmission coefficient T can be obtained using the formula [32]:

$$T = 2n/(n^2 + 1) \quad (9)$$

The listed data in Table 3 show the partial inverse proportionality between R_L and T with increasing sputtered Cu interlayer thickness. The relative density D_r is an important parameter which reflect the degree of crystallization of thin film oxides. The D_r can be calculated based on the average refractive index values of each of the three samples by the following equation [33]

$$D_r = \frac{n^2 - 1}{n_0^2 - 1} \times 100(\%) \quad (10)$$

where n_o is the refractive index of single crystal anatase ZnO. Table 3 presents the value of D_r for $ZC_{20}Z$, $ZC_{50}Z$ and $ZC_{70}Z$. The D_r values increase with increasing film thickness and Cu interlayer thickness as well. This behavior indicates that the crystalline quality of the three films investigated gradually improves with increasing Cu interlayer thickness, as compared with the crystallite size given in Table 1 and the D_r data given in Table 3.

3.5 Optical and electrical conductivities

The difference between the optical and electrical conductivities is that the optical conductivity σ_{opt} involves the dielectric constant while the electrical conductivity σ_e involves the resistivity of the materials. The optical and electrical conductivities for $ZC_{20}Z$, $ZC_{50}Z$ and $ZC_{70}Z$ were calculated according to the expressions given in [34, 35]. Figures 9 and 10 show the variation of σ_{opt} and σ_e as a function of photon energy for the three samples under investigation.

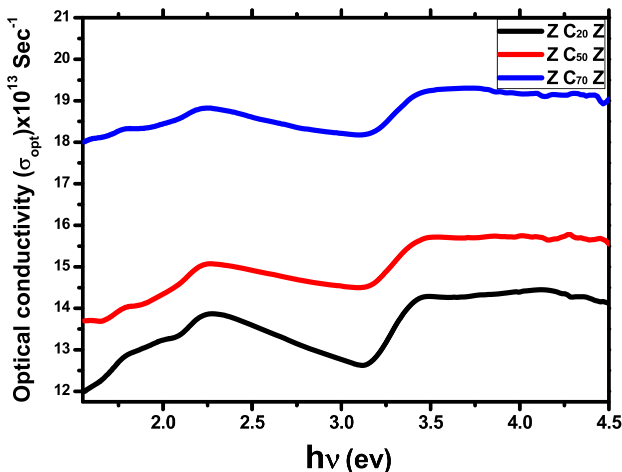

Fig. 9 Optical conductivity versus ($h\nu$) for $ZC_{20}Z$, $ZC_{50}Z$ and $ZC_{70}Z$ thin films grown by ALD

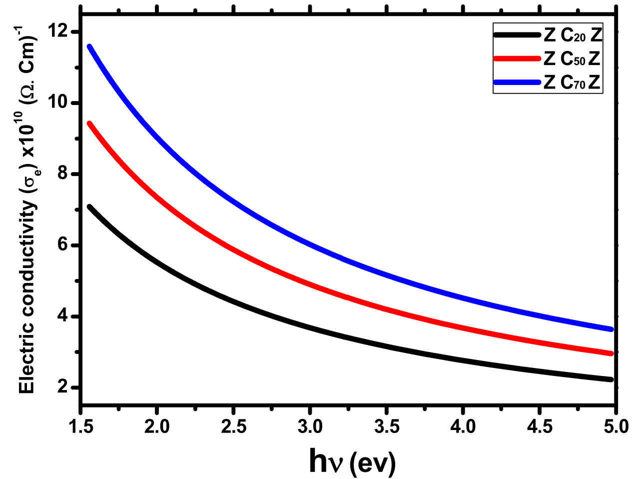

Fig. 10 Electrical conductivity versus ($h\nu$) for $ZC_{20}Z$, $ZC_{50}Z$ and $ZC_{70}Z$ thin films grown by ALD

Analysis of these plots shows an increase in both conductivities with increasing sputtered Cu interlayer thickness. Generally, the energy band gap is directly linked to conductivity; electrical conductivity is inversely proportional to the optical energy gap. This relation was confirmed by comparing the E_g values given in Table 2 with the behavior of the electrical conductivity shown in Fig. 10.

4 Conclusions

To investigate the effect of different thicknesses of sputtered Cu interlayer on surface morphology, crystallinity, surface roughness and optical band gap, three trilayer thin film samples were prepared. The top and bottom 70 nm ZnO thin films were prepared by ALD, while Cu interlayers of different thicknesses (20, 50 and 70 nm) were prepared by sputtering. The GIXRD diffraction measurements confirmed the improvement of the crystallinity of the samples with increasing sputtered Cu interlayer thickness. The absorption spectra for the three films were reported and thoroughly analyzed. Analysis of the results confirmed that the studied ZnO/Cu/ZnO multilayer thin films are appropriate candidates for photocatalysis and sensor device fabrication, and inspire us that ALD is a promising technique for preparing high quality of transparent conducting oxides (TCO) with remarkable optical properties.

Acknowledgements

The samples used in this study were prepared, and films morphology and uniformity were measured at the University of Debrecen, Hungary, according to the agreement between Faculty of Education, Ain Shams University *"Coordinator and Supervisor Prof. Dr. Suzan Fouad"* and Faculty of Science and Technology, University of Debrecen *"Coordinator and Supervisor Prof. Dr. Zoltán Erdélyi"*. The opto-electrical parameters were measured at Laser Physics and Nanotechnology Unit (LPTU), Faculty of Engineering, Shoubra, Benha University. Project no. TKP2021-NKTA-34 has been implemented with the support provided from the National Research, Development and Innovation Fund of Hungary, financed under the TKP2021-NKTA funding scheme.

Author contributions

The submission of the manuscript has been approved by all coauthors. SSF contributed to the idea and the writing and the revision. EB and BP prepared samples. MN measured and calculated the different parameters and revision. SN involved in revision. ZE involved in revision.

Declarations

Conflict of interest The authors declare that they have no known competing financial interests or personal relationships that could have appeared to influence the work reported in this paper.

Data availability The datasets generated during and/or analyzed during the current study are available from the corresponding author on reasonable request.

References

1. Q. Qiao, D. Xu, Y.W. Li, J.Z. Zhang, Z.G. Hu, J.H. Chu, Detection of resistive switching behavior based on the Al_2O_3/ZnO/Al_2O_3 structure with alumina buffers. Thin Solid Films **623**, 8–13 (2017)
2. N. Widiarti, J.K. Sae, S. Wahyuni, Synthesis CuO-ZnO nanocomposite and its application as an antibacterial agent. IOP Conf. Ser. **172**(1), 012036 (2017)
3. H. Zaka, S.S. Fouad, B. Parditka, A.E. Bekheet, H.E. Atyia, M. Medhat, Z. Erdélyi, Enhancement of dispersion optical parameters of Al_2O_3/ZnO thin films fabricated by ALD. Sol. Energy **205**, 79–87 (2020)
4. H.A. Ahmed, S.I. Abu-Eishah, A.I. Ayesh, S.T. Mahmoud, Synthesis and characterization of Cu-doped TiO_2 thin films produced by the inert gas condensation technique. J. Phys: Conf. Ser. **869**(1), 012027 (2017)
5. M.J. Alsultani, H.H. Abed, R.A. Ghazi, M.A. Mohammed, Electrical characterization of thin films (TiO_2: ZnO) 1–x (GO) x/FTO heterojunction prepared by spray pyrolysis technique. J. Phys.: Conf. Ser. **1591**(1), 012002 (2020)
6. S.S. Fouad, B. Parditka, M. Nabil, E. Baradács, S. Negm, H.E. Atyia, Z. Erdélyi, Bilayer number driven changes in polarizability and optical property in ZnO/TiO_2 nanocomposite films prepared by ALD. Optik **233**, 166617 (2021)
7. H. Elshimy, T. Abdallah, The effect of mechanically milled lead iodide powder on perovskite film morphology. Appl. Phys. A **128**(1), 1–14 (2022)
8. S.M. Mali, S.S. Narwade, Y.H. Navale, S.B. Tayade, R.V. Digraskar, V.B. Patil, A.S. Kumbhar, B.R. Sathe, Heterostructural CuO–ZnO nanocomposites: a highly selective chemical and electrochemical NO_2 sensor. ACS Omega **4**(23), 20129–20141 (2019)
9. E.T. Wahyuni, P.Y. Yulikayani, N.A. Aprilita, Enhancement of visible-light photocatalytic activity of Cu-doped TiO_2 for photodegradation of amoxicillin in water. J. Mater. Environ. Sci. **11**(4), 670–683 (2020)
10. H. Elshimy, T. Abdallah, S.A. Abou, Optimization of spin coated TiO_2 layer for hole-free perovskite solar cell. IOP Conf. Ser. **762**(1), 012003 (2020)
11. Z. Xu, G. Duan, Y. Li, G. Liu, H. Zhang, Z. Dai, W. Cai, CuO–ZnO micro/nanoporous array-film-based chemosensors: new sensing properties to H_2S. Chemistry **20**(20), 6040–6046 (2014)
12. Q. Xu, D. Ju, Z. Zhang, S. Yuan, J. Zhang, H. Xu, B. Cao, Near room-temperature triethylamine sensor constructed with CuO/ZnO PN heterostructural nanorods directly on flat electrode. Sens. Actuators B Chem. **225**, 16–23 (2016)
13. W. Maziarz, TiO_2/SnO_2 and TiO_2/CuO thin film nano-heterostructures as gas sensors. Appl. Surf. Sci. **480**, 361–370 (2019)
14. A. Shanmugasundaram, D.S. Kim, T.F. Hou, D.W. Lee, Facile in situ formation of CuO/ZnO pn heterojunction for improved H_2S-sensing applications. J. Sens. Sci. Technol. **29**(3), 156–161 (2020)
15. P. Zaumseil, High-resolution characterization of the forbidden Si 200 and Si 222 reflections. J. Appl. Crystallogr. **48**(2), 528–532 (2015)

16. M. Sajjad, I. Ullah, M.I. Khan, J. Khan, M.Y. Khan, M.T. Qureshi, Structural and optical properties of pure and copper doped zinc oxide nanoparticles. Results Phys. **9**, 1301–1309 (2018)
17. M.I. Ionescu, F. Bensebaa, B.L. Luan, Study of optical and electrical properties of ZnO/Cu/ZnO multilayers deposited on flexible substrate. Thin Solid Films **525**, 162–166 (2012)
18. H.S. Das, G. Roymahapatra, P. Kumar, R. Das, Study the effect of ZnO/Cu/ZnO multilayer structure by RF magnetron sputtering for flexible display applications. ES Energy Environ. **13**, 50–56 (2021)
19. T. Wang, H.P. Ma, J.G. Yang, J.T. Zhu, H. Zhang, J. Feng, S.J. Ding, H.L. Lu, D.W. Zhang, Investigation of the optical and electrical properties of ZnO/Cu/ZnO multilayers grown by atomic layer deposition. J. Alloys Compd. **744**, 381–385 (2018)
20. Y. Chen, Q. Tao, W. Fu, H. Yang, Synthesis of PbS/Ni_2+ doped CdS quantum dots cosensitized solar cells: enhanced power conversion efficiency and durability. Electrochim. Acta **173**, 812–818 (2015)
21. E.G. El-Metwally, E.M. Assim, S.S. Fouad, Optical characteristics and dispersion parameters of thermally evaporated $Ge_{50}In_4Ga_{13}Se_{33}$ chalcogenide thin films. Opt. Laser Technol. **131**, 106462 (2020)
22. S.S. Fouad, B. Parditka, A.E. Bekheet, H.E. Atyia, Z. Erdélyi, ALD of TiO_2/ZnO mutilayers towards the understanding of optical properties and polarizability. Opt. Laser Technol. **140**, 107035 (2021)
23. R.J. Álvaro, N.D. Diana, A.M. María, Effect of Cu on optical properties of TiO_2 nanoparticles. Contemp. Eng. Sci. **10**, 1539–1549 (2017)
24. M. Nabil, S.A. Mohamed, K. Easawi, S.S. Obayya, S. Negm, H. Talaat, M.K. El-Mansy, Surface modification of CdSe nanocrystals: application to polymer solar cell. Curr. Appl. Phys. **20**(3), 470–476 (2020)
25. H. Zaka, B. Parditka, Z. Erdélyi, H.E. Atyia, P. Sharma, S.S. Fouad, Investigation of dispersion parameters, dielectric properties and opto–electrical parameters of ZnO thin film grown by ALD. Optik **203**, 163933 (2020)
26. I.M. El Radaf, S.S. Fouad, A.M. Ismail, G.B. Sakr, Influence of Spray time on the optical and electrical properties of $CoNi_2S_4$ thin films. Mater. Res. Express **5**(4), 046406 (2018)
27. M. Caglar, S. Ilican, Y. Caglar, Influence of dopant concentration on the optical properties of ZnO: in films by sol–gel method. Thin Solid Films **517**(17), 5023–5028 (2009)
28. J.A. Duffy, "Trends in energy gaps of binary compounds: an approach based upon electron transfer parameters from optical spectroscopy. J. Phys. C **13**(16), 2979 (1980)
29. V.P. Guptal, N.M. Ravindra, Phys. Stat. Sol. (B) **100**, 715 (1980)
30. S.K. O'Leary, S.R. Johnson, P.K. Lim, The relationship between the distribution of electronic states and the optical absorption spectrum of an amorphous semiconductor: an empirical analysis. J. Appl. Phys. **82**(7), 3334–3340 (1997)
31. S.S. Fouad, I.M. El Radaf, P. Sharma, M.S. El-Bana, Multifunctional CZTS thin films: structural, optoelectrical, electrical and photovoltaic properties. J. Alloys Compd. **757**, 124–133 (2018)
32. M. Nabil, F. Horia, S.S. Fouad, S. Negm, Impact of Au nanoparticles on the thermophysical parameters of Fe_3O_4 nanoparticles for seawater desalination. Opt. Materiales **128**, 112456 (2022)
33. M. Ohyama, H. Kouzuka, T. Yoko, Sol-gel preparation of ZnO films with extremely preferred orientation along (002) plane from zinc acetate solution. Thin Solid Films **306**(1), 78–85 (1997)
34. G. Helmy, Electrical and optical properties of Sb_2O_3 B_2O_3 Bi_2O_3 TeO_2 glass system. Egypt. J. Phys. **47**(1), 23–29 (2019)
35. I.M. El Radaf, H.Y.S. Al-Zahrani, S.S. Fouad, M.S. El-Bana, Profound optical analysis for novel amorphous Cu_2FeSnS_4 thin films as an absorber layer for thin film solar cells. Ceram. Int. **46**(11), 18778–21878 (2020)

Publisher's Note Springer Nature remains neutral with regard to jurisdictional claims in published maps and institutional affiliations.

Springer Nature or its licensor holds exclusive rights to this article under a publishing agreement with the author(s) or other rightsholder(s); author self-archiving of the accepted manuscript version of this article is solely governed by the terms of such publishing agreement and applicable law.